PROCEEDINGS OF SPIE

SPIEDigitalLibrary.org/conference-proceedings-of-spie

Optical trapping of individual magnetic nanoparticles

Akbar Samadi, Mengting Wang, Yanlian Yang, Lene B. Oddershede

Akbar Samadi, Mengting Wang, Yanlian Yang, Lene B. Oddershede, "Optical trapping of individual magnetic nanoparticles," Proc. SPIE 10723, Optical Trapping and Optical Micromanipulation XV, 107230E (7 September 2018); doi: 10.1117/12.2324124

SPIE.

Event: SPIE Nanoscience + Engineering, 2018, San Diego, California, United States

Invited Paper

Optical trapping of individual magnetic nanoparticles

Akbar Samadi[a], Mengting Wang[b], Yanlian Yang[b], and Lene B. Oddershede[a]

[a]Niels Bohr institute, University of Copenhagen, Blegdamsvej 17, 2100 Copenhagen, Denmark.
[b]National Center for Nanoscience and Technology, 11 ZhongGuanCun BeiYiTiao, 100190 Beijing, P.R. China

ABSTRACT

Due to their unique properties, magnetic nanoparticles, often made of iron oxides, have received significant attention in chemistry, solid state physics, and the life sciences. Although a magnetic field is the most obvious mean by which one can manipulate magnetic nanoparticles, we here demonstrate that magnetic nanoparticles can be individually controlled by optical manipulation. We quantify the interaction of optically trapped individual magnetic nanoparticles with the electrical field by determining the spring constant. Also, by finite element modeling we determine the extinction, scattering and absorption cross sections of magnetic nanoparticles as well as the real and imaginary parts of their complex polarizability. In comparison to magnetic manipulation, optical manipulation has the advantage, due to the tight focusing of the laser beam, that it allows for manipulation of a single particle at a time. Also, one can imagine applications where it is advantageous to employ both magnetic and optical manipulations simultaneously.

Keywords: Optical trapping, magnetic nanoparticle, maghemite, Fe_2O_3, optical cross-sections, polarizability

1. INTRODUCTION

Maghemite (γ-Fe_2O_3), one of the most common forms of iron oxides, is a commonly used material for magnetic nanoparticles which can be manipulated and heated by magnetic fields.[1] Due to their low toxicity and favorable biocompatibility, maghmite nanoparticles have found applications in bioengineering and biomedicine, for instance as nanoscale biosensors, as agents for magnetic resonance imaging (MRI) in vivo, as vehicles for controlled delivery and release of drugs, and for magnetic hyperthermia that can be induced by oscillating magnetic fields and used for cancer treatment.[1–3]

Magnetic nanoparticles are, for good reasons, most often thought of as magnetic, and seldom as plasmonic nanoparticles, although they do share chemical and physical properties with other metallic- and metal-oxide nanoparticles. Due to their plasmonic nature, metallic nanoparticles will absorb part of an incident laser beam, in particular at wavelengths close to the particle's resonance, and release the energy in the form of heat in the surrounding medium. Also, at certain wavelengths, they scatter a significant part of an incoming laser beam. Increased absorption and scattering makes it more challenging to optically trap a metallic nanoparticle. Compared to similarly sized dielectric particles, metallic nanoparticles have higher polarizability, thus nevertheless enabling optical trapping which has been reported for gold,[4] silver,[5,6] and platinum nanoparticles[7] of various shapes[8] and sizes.[9] Micron-sized dielectric polystyrene particles with a coating of magnetic material have been reported optically manipulated by cylindrical laser beams[10] and by Bessel-Gaussian beams.[11]

For biological applications, lasers with wavelengths in the near-infrared (NIR) are often chosen because biological tissue is largely transparent to NIR irradiation. Upon NIR laser irradiation, the temperature of metallic nanoparticles can easily increase by hundreds of degrees of Celsius.[12,13] This property makes plasmonic nanoparticles quite favorable for laser induced thermoplasmonic cancer treatment[13–15] as well as for controlled cell fusion[16,17] or for controlled cargo release.[18] These applications are all parallel to the applications of magnetic nanoparticles, lined out in the beginning of this introduction, controlled by a magnetic field.

Further author information: (Send correspondence to Lene B. Oddershede)
L. B. O.: E-mail: oddershede@nbi.ku.dk, Telephone: +45 24942534

Optical Trapping and Optical Micromanipulation XV, edited by Kishan Dholakia, Gabriel C. Spalding, Proc. of SPIE Vol. 10723, 107230E · © 2018 SPIE · CCC code: 0277-786X/18/$18 · doi: 10.1117/12.2324124

Using a simple focused Gaussian laser beam, a standard optical trap, we here show that it is possible to optically trap individual solid magnetic nanoparticles in 3D. At several laser powers we experimentally quantify the spring constant characterizing the strength of the harmonic optical trapping potential. In parallel, we use finite element modeling (FEM) to calculate the polarizability and the optical cross-sections of the magnetic nanoparticles in a spectrum ranging from the UV to NIR wavelengths and find that the calculated extinction cross-sections agree with the measured ones. These results significantly broaden the use of magnetic nanoparticles which can be manipulated both by magnetic and electric fields and which have a significant absorption of NIR laser light, thus making them prone candidates also for laser activated photothermal therapy.

2. EXPERIMENTAL METHODS

Optical tweezers

The optical tweezers setup were implemented in an inverted microscope (Leica DMIRB HC) and based on a NIR CW laser (Nd: YVO4, 5 W Spectra Physics Millennia, λ=1064 nm) with a Gaussian intensity profile. The laser was steered into the microscope via a backport of the microscope. The laser was tightly focused into a diffraction limit spot using an oil immersion objective (HCX, PL, APO, 100/NA = 1.4). To minimize spherical aberration and obtain optimum trapping efficiency at depth of 5 μm from the lower glass surface of the chamber, we used an immersion oil with index of refraction n = 1.54 on the objective.[19] The trapping laser light was focused by a condenser after passing the sample and imaged onto a quadrant photodiode (QPD) (S5981, Hamamatsu) located at the back focal plane of the condenser. The condensers aperture was set to an optimized opening in order to obtain better signal to noise ratio.[20,21] Data acquired by the QPD was transferred to the PC via a DAQ card (CB-68LP, National Instruments). The subsequent time-series analyses were performed using custom-made Labview programs. A CCD camera (Sony XC-EI50 - 25 Hz frame rate) was utilized for bright field imaging based on back-scattered light from the trapped nanoparticle, this was useful for navigating in the sample and for ensuring that only a single particle was trapped during the measurements. The chamber was mounted on a 3D piezoelectric stage (PI 731.20, Physik Instrumente, Germany) enabling nanometer accuracy positioning of the chamber with reference to the trap position. A schematic illustration of optical tweezers set up is shown in figure 1a.

Preparation and characterization of the magnetic nanoparticles

Maghemite (Fe_2O_3) nanoparticles were purchased from Ademtech, France. The nanoparticles were diluted in milliQ water (100X) and sonicated for at least 15 min. After this, the solution was filter-sterilized through membrane pore sizes of 400 nm to eliminate or minimize aggregates. In preparation for the trapping experiments, the suspension with magnetic nanoparticles was flushed into a perfusion chamber made of a cover glass attached to a microscope slide using one layer of double-sided sticky scotch tape as spacers between the two glass surfaces.

The manufacturer (Ademtech, France) states that the mean diameter of the maghemite particles is 220-250 nm. As the size of a trapped nanoparticle has a major impact on its optical cross-sections and the trap stiffness, we performed an independent size check using a Dynamic Light Scattering (DLS) machine (Malvern Zetasizer Nano ZS90). The size distribution obtained from the DLS measurements is shown in figure 1b. The peak of the distribution is around d=235 nm, and this number is in very good agreement with the interval stated by the manufacturer. Hence, in the following we assume the diameter of the magnetic particles to be d=235 nm.

3. FINITE ELEMENT MODELING (FEM)

Optical Cross-Sections

In order to characterize the optical properties of the magnetic nanoparticles and thereby quantify their interaction with light, we have performed FEM using relevant packages from COMSOL (Stockholm, Sweden). In order to obtain the electric field, $\mathbf{E}=\mathbf{E_{inc}}+\mathbf{E_{scat}}$, satisfying the boundary conditions, we numerically solved Maxwell's wave equation in the frequency domain. The obtained electric field was then used to calculate the scattering and absorption cross-sections using the following equations:[7]

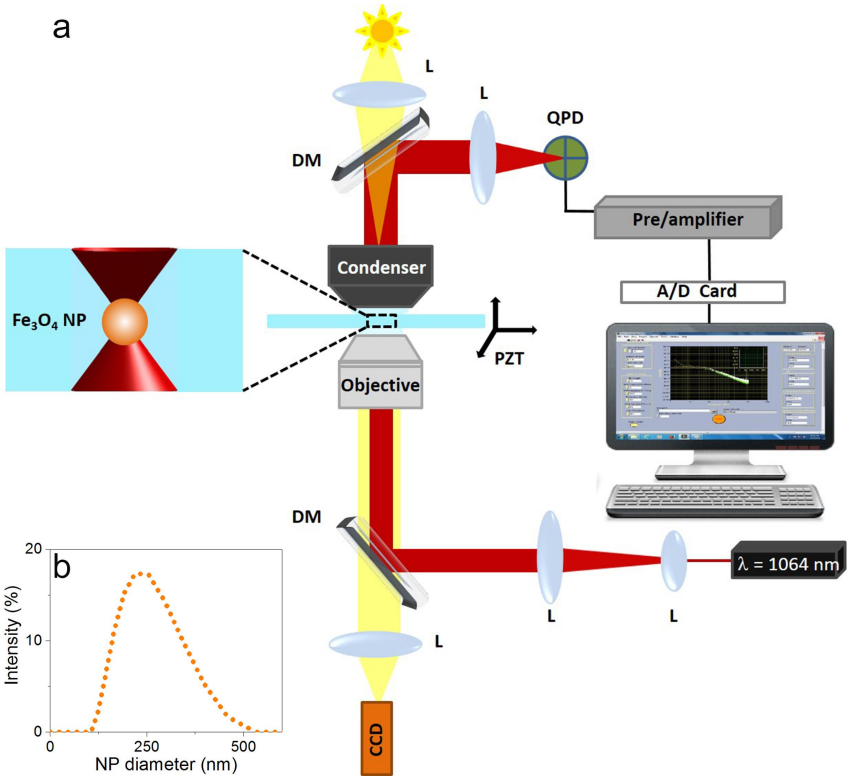

Figure 1. (a) Schematic of the optical tweezers setup used for trapping of magnetic (Fe_2O_3) nanoparticles. An expanded $\lambda = 1064$ nm laser beam is coupled into a microscope objective using a Dichroic Mirror (DM) and a couple of lenses (L). The zoom-in shows the sample where a magnetic particle is trapped at the focus of the objective. (b) Size distribution of the magnetic particles measured by Dynamic Light Scattering (DLS), the measured mean diameter is d=235 nm.

$$\sigma_{\mathbf{scat}} = \frac{2}{c\epsilon_0|\mathbf{E_{inc}}|^2}\int\int(\mathbf{n}\cdot\mathbf{S_{scat}})dS = \frac{1}{c\epsilon_0|\mathbf{E_{inc}}|^2}\int\int(\mathbf{n}\cdot Re[\mathbf{E_{scat}}\times\mathbf{H_{scat}}^*])dS \quad (1)$$

$$\sigma_{\mathbf{abs}} = \frac{2}{c\epsilon_0|\mathbf{E_{inc}}|^2}\int\int\int qdV = \frac{2}{c\epsilon_0|\mathbf{E_{inc}}|^2}\int\int\int\frac{1}{2}Re[\mathbf{J}\cdot\mathbf{E}^*]dV \quad (2)$$

where $\mathbf{S_{scat}}=\frac{1}{2}Re[\mathbf{E_{scat}}\times\mathbf{H_{scat}}^*]$ and $q=\frac{1}{2}Re[\mathbf{J}\cdot\mathbf{E}^*]$ are the scattered Poynting vector and the electromagnetic power loss density within the nanoparticle, respectively. Complex conjugation is marked with an asterisk. The extinction cross-section is a sum of the scattering and absorption cross-sections and can be written as $\sigma_{ext}=\sigma_{scat}+\sigma_{abs}$. All optical constants needed to perform this calculation were taken from RefractiveIndex.info

website.[22] Importantly, optical constants for γ-Fe_2O_3 were not available, instead in the FEM we used the optical constants for α-Fe_2O_3. Details on the FEM can be found in.[7]

In addition to calculating the extinction cross section, σ_{ext}, we directly measured it using UV-VIS spectrophotometry. The experimentally measured extinction cross section as a function of wavelength for 235 nm magnetic nanoparticles is shown in figure 2a. The optical cross sections as a function of wavelength calculated by FEM are shown in figure 2b; σ_{ext} by a full black line, σ_{abs} by a dashed red line, and σ_{scat} by a dotted blue line, respectively. The experimentally obtained extinction cross-sections of a 235 nm magnetic nanoparticle shown in figure 2a can be directly compared to the FEM-based calculated extinction cross-section (solid black line) in figure 2b.

Polarizability and optical forces

In the Rayleigh regime, the size of particle is much smaller than the wavelength of the incoming electromagnetic field. In this regime, the gradient force, exerted by the optical trap and responsible for trapping, is linearly proportional to the polarizability of the trapped particle:[5,7]

$$\mathbf{F}_{grad} = \frac{1}{4}\alpha_r \nabla \langle |\mathbf{E}|^2 \rangle \tag{3}$$

The complex polarizability of a nanoparticle, α=α_r+ iα_i, is related to the optical cross-sections in the following manner:

$$\sigma_{abs} = \frac{k}{\epsilon_0}\alpha_i \tag{4}$$

$$\sigma_{scat} = \frac{k^4}{6\pi\epsilon_0^2}|\alpha|^2 \tag{5}$$

where $k = \frac{2\pi n_m}{\lambda_0}$ is the wavenumber with n_m being the refractive index of the surrounding medium. λ_0 and ϵ_0 are the wavelength and permittivity in vacuum, respectively.

Figure 3a shows the real, α_r (blue), and imaginary, α_i (red), parts of the complex polarizability as a function of wavelength calculated by FEM for a 235 nm magnetic particle. At a wavelength of 1064nm, as used in the experiments, the numerical values of the polarizability are $\alpha_r = 9.7\times10^{-32}$ $(F\cdot m^2)$ and $\alpha_i = 1.2\times10^{-33}$ $(F\cdot m^2)$.

As visible from figure 3a, α_r is positive for all depicted wavelengths. As the gradient force, $\mathbf{F}_{grad}$ is proportional to α_r, this means that magnetic NPs should be optically trappable at all wavelengths between 300 nm and 1200 nm. Figure 3b shows the normalized amplitude of the electromagnetic field at λ=1064 nm around an irradiated magnetic nanoparticle calculated by FEM. The double-headed arrow shows the polarization direction of the linearly polarized incident electric field and the induced electrical dipole is clearly visible.

4. OPTICAL TRAPPING OF MAGNETIC NANOPARTICLES

As expected on the basis of the results shown in figure 3 we were indeed able to optically trap individual magnetic nanoparticles. The number of particles in the trap was determined both by visual inspection and by the width of the positional histograms (shown in the inset of figure 4a) as done, e.g., in Ref.4. For small displacements of a trapped particle around the equilibrium position of the trap, the position histograms are Gaussian and the optical force exerted on the particle can be treated as a Hookean force: $\mathbf{F}_{trap} = -\kappa x$ where κ is the spring constant characterizing the optical trapping potential and x is the deviation from the equilibrium position. The dynamics of the trapped particle is well described by the Langevin equation:

$$ma(t) = -\gamma v(t) - \kappa x(t) + \mathcal{F}_t(t). \tag{6}$$

Here, m is the mass of trapped particle, $a(t)$ its acceleration, $v(t)$ its velocity, γ is the friction coefficient, and $\mathcal{F}_{thermal}(t)$ is a stochastic time-dependent force originating from the thermal collisions with the solvent molecules.

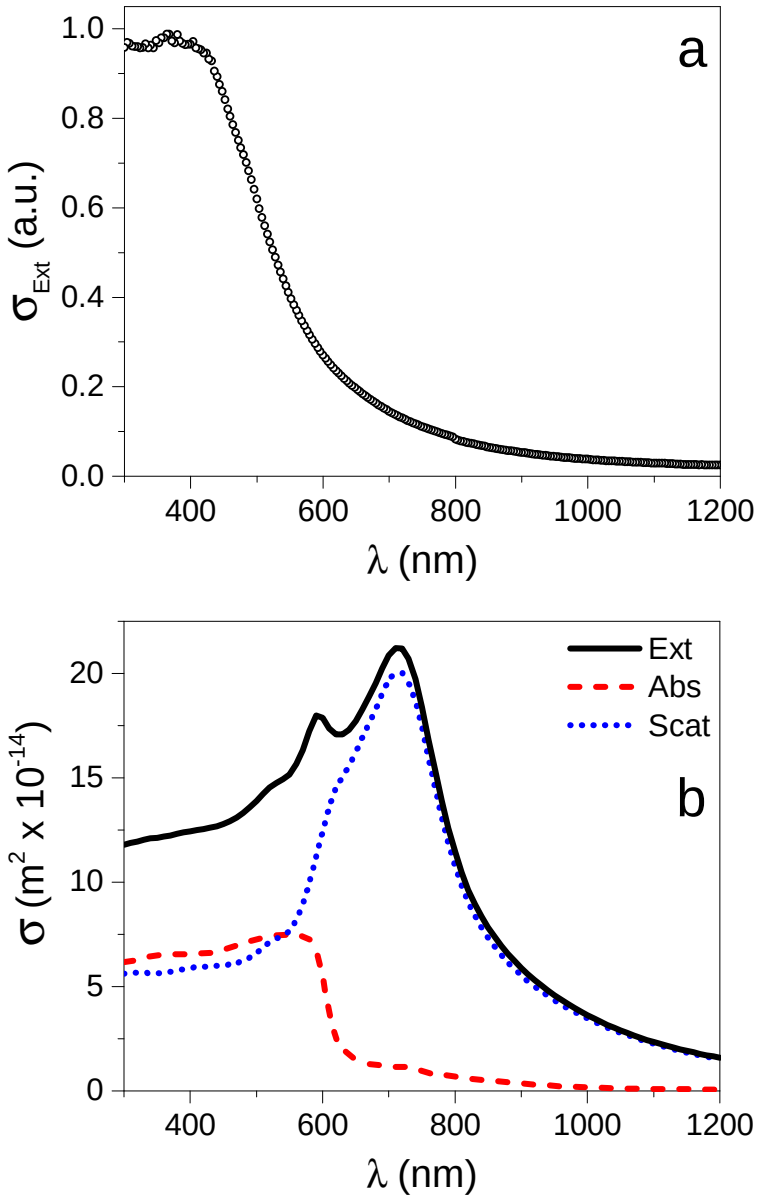

Figure 2. Characterization of the optical properties of a 235 nm magnetic particle. (a) Experimentally measured extinction cross-section of magnetic nanoparticles in bulk solution obtained by UV-VIS spectrophotometri. (b) Extinction (full black line), absorption (dashed red line) and scattering (dotted blue line) cross-sections as a function of wavelength obtained by finite element modeling.

As the Reynolds number describing the particle's dynamics is so low that the inertial term is negligible compared to the other terms, equation 6 can be set equal to zero. The Langevin equation can then be Fourier transformed and the positional power spectrum can be calculated:

$$P(f) = |x(f)|^2 = \frac{k_B T}{\gamma} \frac{1}{(f^2 + f_c^2)}. \tag{7}$$

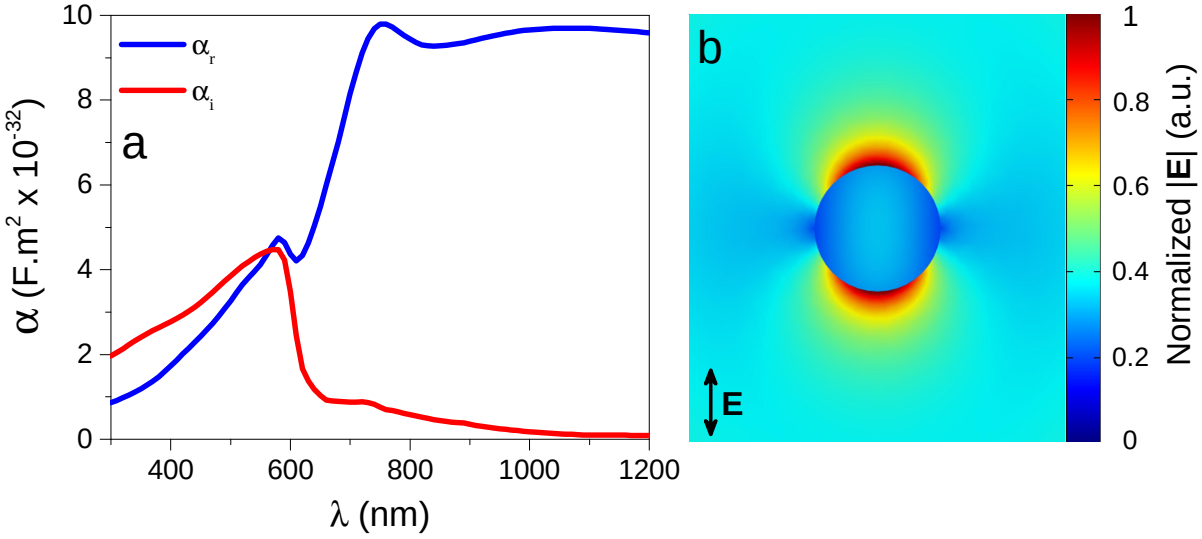

Figure 3. Polarizability and electric field around an optically trapped 235 nm magnetic particle calculated by FEM. (a) Real (full blue line) and imaginary (full red line) parts of the complex polarizability of the nanoparticle as a function of wavelength. (b) Normalized electric field amplitude around the nanoparticle under illumination of a linearly polarized plane wave with $\lambda = 1064$ nm.

Here, f_c is the corner frequency of the system which is defined as $\kappa = 2\pi\gamma f_c$. For a spherical particle the Stokes-Einstein equation gives $\gamma = 6\pi\eta R$, with η being the viscosity of water and R the radius of the trapped particle.

The experimentally acquired time series of individually trapped magnetic nanoparticles were Fourier transformed and fitted by the theoretically expected power spectrum (equation 7) using MatLab routines[23] taking the filtering effect of the QPD into account.[24] By fitting equation 7 to the experimental data and recalling the definition of f_c, κ can be obtained.

Examples of power spectra in lateral directions perpendicular to the laser's polarization (y) and parallel to the laser's polarization (x) are shown in figure 4a. Full lines show fits by equation 7 to the data and the insets show the positional histograms, the full lines are fits by Gaussian functions. The experimentally obtained spring constants, κ, which differ in the translational directions, are shown in figure 4 as a function of laser power. For an optical trap based on a Gaussian laser beam, κ is significantly weaker in the axial direction than in the lateral directions. Also, for the particle sizes relevant in the current study, the trap is usually stronger perpendicular to the laser's polarization direction (y-direction in the current study) than parallel to the polarization (x-direction).[25] These expected features are all present in the data originating from optical trapping of single magnetic particles. Also worth noticing is the fact that the spring constants are linearly proportional to laser power, which is a hallmark of optical trapping.

To our knowledge, this is the first reported optical trapping of solid magnetic particles. The spring constants here obtained here from 235 nm solid magnetic particles are about 2-3 times smaller than those obtained for micron-sized polystyrene particles coated by a magnetic shell.[10] The volumes of the magnetic nanoparticles here studied are more than a factor of 100 smaller than the particles studies in Ref.10, hence, a massive magnetic nanoparticle seems more easily trappable (per volume) than magnetic shells with polystyrene cores.

5. CONCLUSION

We optically trapped individual massive magnetic nanoparticles in three dimensions using a tightly focused NIR Gaussian laser beam. Using finite element modeling we calculated their optical cross-sections and as

well as their polarizability as a function of wavelength. In the visible and near-infrared spectrum the real part of the polarizability of 235 nm magnetic nanoparticles was positive, thus inferring that these particles should be trappable in this large spectrum of light. By analyzing the thermal fluctuations of the trapped particles, we quantified the spring constants characterizing the stiffness of the harmonic trapping force. These results prove that magnetic nanoparticles, which can be controlled and manipulated by magnetic fields, can also be manipulated by electric fields and even optically trapped relatively firmly compared to other similarly sized particles. This paves the road for novel opportunities in nano-manipulation and exploitation of magnetic nanoparticles.

REFERENCES

[1] Zia, M., Phull, A. R., and Ali, J. S., "Synthesis, characterization, applications, and challenges of iron oxide nanoparticles," *Nanotechnol. Sci. Appl.* **9**, 49–67 (2016).

[2] Kumar, A. and Gupta, M., "Synthesis and surface engineering of iron oxide nanoparticles for biomedical applications," *Biomaterials* **26**, 3995–4021 (2005).

[3] Mohapatra, M. and Anand, S., "Synthesis and applications of nano-structured iron oxides / hydroxides a review," *Int. J. Eng. Sci.* **2**, 127–146 (2010).

[4] Hansen, P. M., Bhatia, V. K., Harrit, N., and Oddershede, L., "Expanding the optical trapping range of gold nanoparticles," *Nano Lett.* **5**, 1937–1942 (2005).

[5] Svoboda, K. and Block, S. M., "Optical trapping of metallic Rayleigh particles," *Opt. Lett.* **19**, 930–932 (1994).

[6] Bosanac, L., Aabo, T., Bendix, P. M., and Oddershede, L. B., "Efficient optical trapping and visualization of silver nanoparticles," *Nano Lett.* **8**, 1486–1491 (2008).

[7] Samadi, A., Bendix, P. M., and Oddershede, L. B., "Optical manipulation of individual strongly absorbing platinum nanoparticles," *Nanoscale* **9**, 18449–18455 (2017).

[8] Selhuber-Unkel, C., Zins, I., Schubert, O., S onnichsen, C., and B., O. L., "Quantitative Optical Trapping of Single Gold Nanorods," *Nano. Lett.* **8**, 2998–3003 (2008).

[9] Bendix, P. M., Jauffred, L., Norregaard, K., and Oddershede, L. B., "Optical Trapping of Nanoparticles and Quantum Dots," *IEEE J. Sel. Top. Quantum Electron.* **20**, 4800112–4800112 (2014).

[10] Zhong, M.-C., Gong, L., Li, D., J.-H., Z., Z.-Q., W., and Y.-M., L., "Optical trapping of core-shell magnetic microparticles by cylindrical vector beams," *Appl. Phys. Lett.* **32**, 181112 (2014).

[11] Gong, L., Liu, W., Zhao, Q., Ren, Y., Qiu, X., Zhong, M., and Li, Y., "Controllable light capsules employing modified bessel-gauss beams," *Scientific Reports* **6**, 29001 (2016).

[12] Bendix, P. M., Reihani, S. N., and Oddershede, L. B., "Direct measurements of heating by electromagnetically trapped gold nanoparticles on supported lipid bilayers," *ACS Nano* **4**(4), 2256–2262 (2010).

[13] Samadi, A., Klingberg, H., Kjær, A., Martin, P., and Oddershede, L. B., "Platinum nanoparticles: a non-toxic, effective and thermally stable alternative plasmonic material for cancer therapy and bioengineering," *Nanoscale* **10**, 9097–9107 (2018).

[14] Jørgensen, J. T., Norregaard, K., Tian, P., Bendix, P. M., Kjaer, A., and Oddershede, L. B., "Single particle and pet-based platform for identifying optimal plasmonic nano-heaters for photothermal cancer therapy," *Sci. Rep.* **6**, 30076 (2016).

[15] Jorgensen, J., Norregaard, K., Martin, M., Oddershede, L., and Kjaer, A., "Non-invasive early response monitoring of nanoparticle-assisted photothermal cancer therapy using 18f-fdg, 18f-flt, and 18f-fet pet/ct imaging," *Nanotheranostics* **2**(3), 201–210 (2018).

[16] Rorvig-Lund, A., Bahadori, A., Semsey, S., Bendix, P. M., and Oddershede, L. B., "Vesicle fusion triggered by optically heated gold nanoparticles," *Nano Lett.* **15**(6), 4183–4188 (2015).

[17] Bahadori, A., Oddershede, L. B., and Bendix, P. M., "Hot nanoparticle mediated fusion between selected cells," *Nano Research* **10**(6), 2034–2045 (2017).

[18] Huschka, R., Zuloaga, J., Knight, M. W., Brown, L. V., Nordlander, P., and Halas, N. J., "Light-induced release of dna from gold nanoparticles: Nanoshells and nanorods," *J. Am. Chem. Soc.* **133**(31), 12247–12255 (2011).

[19] Reihani, S. and Oddershede, L. B., "Optimizing immersion media refractive index improves optical trapping by compensating spherical aberrations," *Opt. Lett.* **32**(14), 1998–2000 (2007).
[20] Dreyer, J. K., Berg-Sørensen, K., and Oddershede, L., "Improved axial position detection in optical tweezers measurements," *Appl. Opt.* **43**, 1991–1995 (2004).
[21] Samadi, A. and Reihani, S. N. S., "Role of condenser iris in optical tweezer detection system," *Opt. Lett.* **36**, 4056–4058 (2011).
[22] M. N. Polyanskiy, "Refractive index database, https://refractiveindex.info."
[23] Martin, P. and Toli, I. M., "tweezercalib 2 . 0 : Faster version of MatLab package for precise calibration of optical tweezers ," *Comput. Phys. Commun.* **174**, 518–520 (2006).
[24] Berg-Sørensen, K., Oddershede, L., Florin, E., and Flyvbjerg, H., "Unintended filtering in typical photodiode detection system for optical tweezers," *Journal of Applied Physics* **93**, 3167–3176 (2003).
[25] Madadi, E., Samadi, A., Cheraghian, M., and Reihani, S. N. S., "Polarization-induced stiffness asymmetry of optical tweezers," *Opt. Lett.* **37**, 3519–3521 (2012).

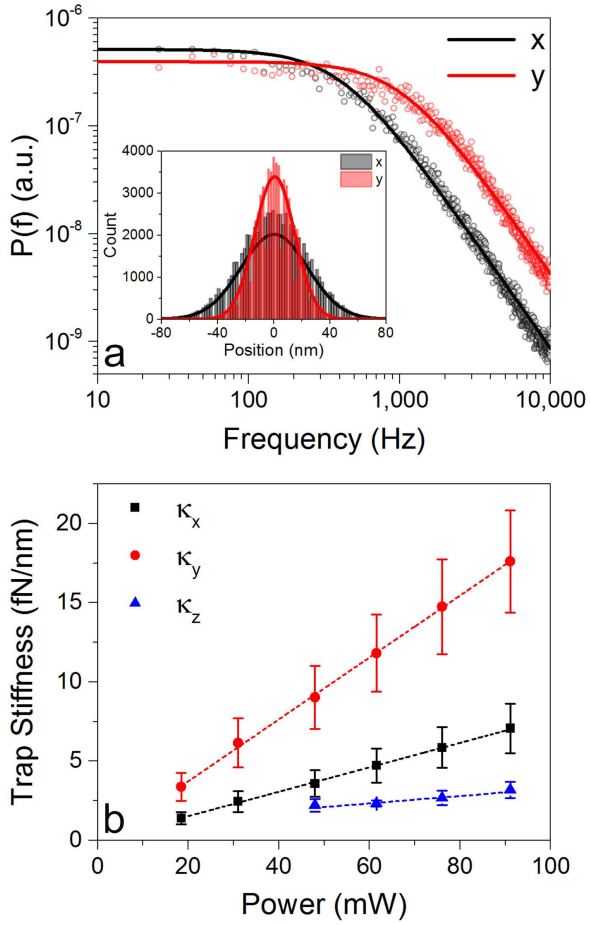

Figure 4. (a) Power spectrum, P(f), of a d=235 nm trapped magnetic NP in x-direction (along laser polarization-black color) and y-direction (perpendicular to the laser polarization-red color) for a used laser power, P=91 mW at sample plane of oil immersion objective, NA=1.4, (corresponding to the last data point in graph b), the inset shows the visited positions distribution of trapped NP within the trap. (b) Measured stiffnesses of trapped NP as a function of used laser power at the sample plane. The black squares, red circles, and blue triangles show the measured data along x, y and z directions, respectively. Each data point represents an average of N=10 different measurements and error bars show one standard deviation. The dashed lines are linear fits to the obtained data.